Technetium Waste Form Development –Progress Report

Fuel Cycle Research & Development

Prepared for
U.S. Department of Energy
Separations/Waste Form Campaign

E. C. Buck
Pacific Northwest National Laboratory

February, 2010

FCR&D-PN0915030312
PNNL-19195

DISCLAIMER

This information was prepared as an account of work sponsored by an agency of the U.S. Government. Neither the U.S. Government nor any agency thereof, nor any of their employees, makes any warranty, expressed or implied, or assumes any legal liability or responsibility for the accuracy, completeness, or usefulness, of any information, apparatus, product, or process disclosed, or represents that its use would not infringe privately owned rights. References herein to any specific commercial product, process, or service by trade name, trade mark, manufacturer, or otherwise, does not necessarily constitute or imply its endorsement, recommendation, or favoring by the U.S. Government or any agency thereof. The views and opinions of authors expressed herein do not necessarily state or reflect those of the U.S. Government or any agency thereof.

SUMMARY

The DOE Fuel Cycle Research & Development (FCR&D) Program is developing aqueous and electrochemical approaches to the processing of used nuclear fuel that will generate technetium-bearing waste streams. This report presents Pacific Northwest National Laboratory (PNNL) research to evaluate an iron-based alloy waste form for Tc that provides high waste loading within waste form processing limitations, meets waste form performance requirements for durability and the long-term retention of radionuclides, and can be produced with consistent physical, chemical, and radiological properties that meet regulatory acceptance requirements for disposal.

Microanalysis with scanning electron microscopy (SEM) was used to analyze a non-radioactive FeMo-Re sample. The Transmission Electron Microscope (TEM) was not functional and, therefore, only preliminary SEM work can be reported. The results are in agreement with previous studies (Ebert et al., 2009 and Frank et al., 2009).

CONTENTS

Contents

1. INTRODUCTION 1

2. RESULTS 3
2.1 Scanning Electron Microscopy of the FeMo-Re alloy 3
2.2 TEM sample preparation 7

3. CONCLUSIONS 14

4. REFERENCES 15

Appendix A 17

Appendix B 18

FIGURES

Figure 1.1Photograph of 48Fe-38Mo-14Re (FeMo-Re alloy). The diameter of the ingot was about 2 cm [image taken from Frank et al., 2009]. 2

Figure 2.1 SEM analysis of FeMo-Re alloy; (a) iron map, (b) molybdenum map, (c) rhenium map, and (d) backscattered electron image. 3

Figure 2.2 SEM analysis of FeMo-Re alloy; (a) iron map, (b) molybdenum map, (c) rhenium map, and (d) backscattered electron image. 4

Figure 2.3 SEM analysis of FeMo-Re alloy; The RGB combination map used a mixture of elemental maps; iron, rhenium, and molybdenum. The instrument generated a map with Zr although Zr is not present in the alloy. 5

Figure 2.4 EDS of different phase compositions in the FeMo-Re alloy. 5

Figure 2.5 Backscattered images of FeMo-Re alloy showing a higher average Z material in the center of the Mo-Re rich regions. 6

Figure 2.6 SEM analysis of FeMo-Re alloy, including a combination map, iron map, molybdenum map, rhenium map, and backscattered electron (BSE) image. 6

Figure 2.7 Series of data analyses showing variation in iron content. 7

Figure 2.8 SEM image of specimen to be examined with TEM. 8

ACRONYMS

BSE	Backscattered Electron
EBR-II	Experimental Breeder Reactor-II
FCR&D	Fuel Cycle Research & Development
INL	Idaho National Laboratory
PNNL	Pacific Northwest National Laboratory
SEM	Scanning electron microscopy
TEM	Transmission electron microscopy

Technetium Waste Form Development – Progress Report

1. INTRODUCTION

Recycling of used nuclear fuel offers some significant advantages over direct disposal, yet the environmental issues associated with the waste forms created are unlikely to disappear. While these advanced waste forms may occupy considerably smaller volumes than previously developed waste forms, a repository may still be required for their ultimate disposal, whether this be in the form of long-term geological repository or a monitored storage facility. The behavior of the advanced waste forms need to be evaluated in terms of the full range of environmental conditions that are possible within a repository setting. Changes in environmental conditions are expected, and may originate from the waste forms themselves (e.g., heat, radiation damage, waste form corrosion), or may reflect the natural variability of the repository setting (e.g., water seepage rates, mechanical stability). In some cases, the environmental setting may directly reflect the durability of the waste form itself. It is important to have a good understanding of the microstructure of the waste forms to develop effective long-term models for corrosion and to build scientific basis for the disposal strategy.

Metallic waste forms were previously developed by Idaho National Laboratory (INL) for EBR-II wastes (Abraham et al., 2001). The minimum additive waste stabilization (MAWS) approach is being utilized to produce a metal waste form that both addresses the performance acceptance requirements and minimizes the amount of additional materials that needs to be added to make a durable material. In this project, a 48wt% Fe, 38 wt% Mo, with 14 wt% Re alloy (termed FeMo-Re alloy) and a 52 wt% Fe, 41 wt% Mo with 7 wt% Tc (termed FeMo-Tc alloy) were prepared at INL. Both samples were received at PNNL for further analyses with electron microscopy. Unlike the metals examined in the last campaign reported in Gelles et al. (2009), these materials did not contain zirconium.

Figure 1.1Photograph of 48Fe-38Mo-14Re (FeMo-Re alloy). The diameter of the ingot was about 2 cm [image taken from Frank et al., 2009].

Initial XRD and SEM analyses at INL indicated both materials were multi-phase alloys. The XRD revealed differences between the FeMo-Re alloy and the FeMo-Tc alloy. Un-dissolved molybdenum was observed in the FeMo-Re alloy. The effects of processing time and heat treatments on the microstructure and phase compositions need to be determined as part of the metal waste form alloy development. In this study, only the FeMo-Re alloy was analyzed and only the SEM analyses are reported as the TEM was available owning to system failures.

As was found during analyses reported by Frank and co-workers (Frank et al., 2009), three phases were detected: An almost pure molybdenum phase which was thought to be residual metallic molybdenum wire that did not completely dissolve; an iron-rich phase, and a rhenium-rich iron phase. The appropriate phase diagrams (Frank et al., 2009) suggest that the rhenium-rich phase and α-Fe (ferrite) phase with molybdenum will be stable between 1488 °C and 1200 °C. As the alloy cooled below 1200 °C, solid state diffusion may have been too slow to convert the rhenium-rich phase to another form that is thermodynamically more stable than the rhenium phase at lower temperatures and has slightly lower molybdenum content. The lever rule predicts the rhenium-rich phase should be present in greater abundance than the ferrite solid solution. These

predictions are borne out in the characterization studies reported here and elsewhere (Ebert et al., 2009).

2. RESULTS

2.1 Scanning Electron Microscopy of the FeMo-Re alloy

Several images and elemental maps were obtained together with x-ray energy dispersive spectroscopy (EDS) analyses of the FeMo-Re alloy. Elemental maps were also obtained that show the nature of the alloy phase. The magnification scale was checked against a standard (see Appendix A).

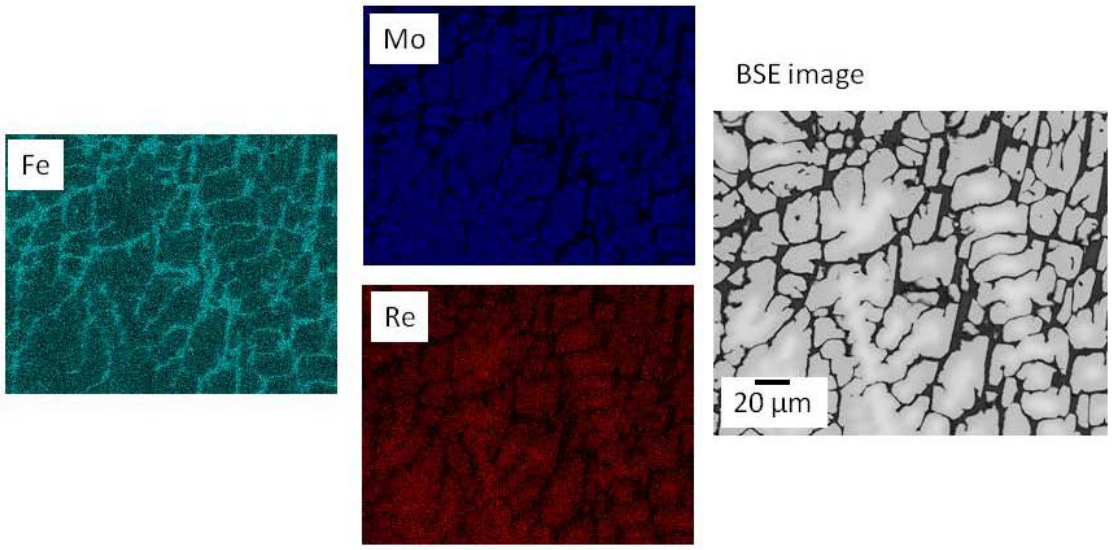

Figure 2.1 SEM analysis of FeMo-Re alloy; (a) iron map, (b) molybdenum map, (c) rhenium map, and (d) backscattered electron image.

The Fe-Re phase diagram suggests that an intermetallic phase (η) will form initially and will equilibrate (and dissolve into) first with δ-Fe and then remain dissolved in the γ-Fe that forms to replace the δ-Fe (Ebert et al., 2009). Instead of forming the η-Fe-Re intermetallic phase, the rhenium appears to substitute into a FeMo intermetallic phase. In Figures 2.1 and 2.2, the SEM

images and elemental maps show the presence of these phases. There is a need to determine the nature of the iron phases but this cannot be determined without the structural analysis capabilities of TEM.

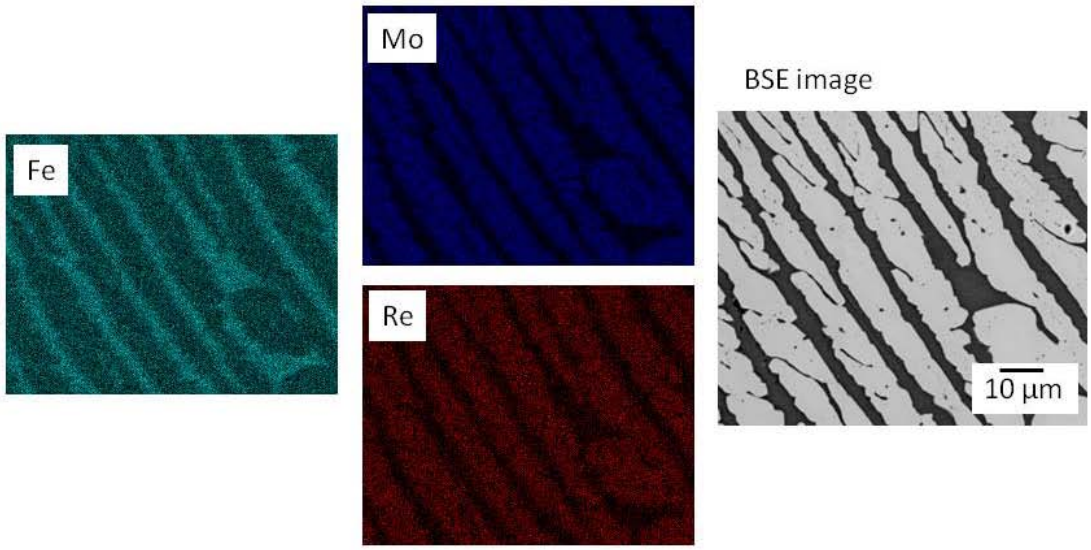

Figure 2.2 SEM analysis of FeMo-Re alloy; (a) iron map, (b) molybdenum map, (c) rhenium map, and (d) backscattered electron image.

In Figure 2.3, a concentrated region of molybdenum metal is shown. This feature was uncommon in the material and may be due to un-dissolved molybdenum wire as suggested by Frank et al. (2009). Adjacent to this molybdenum region, the rhenium was higher in concentration relative to iron.

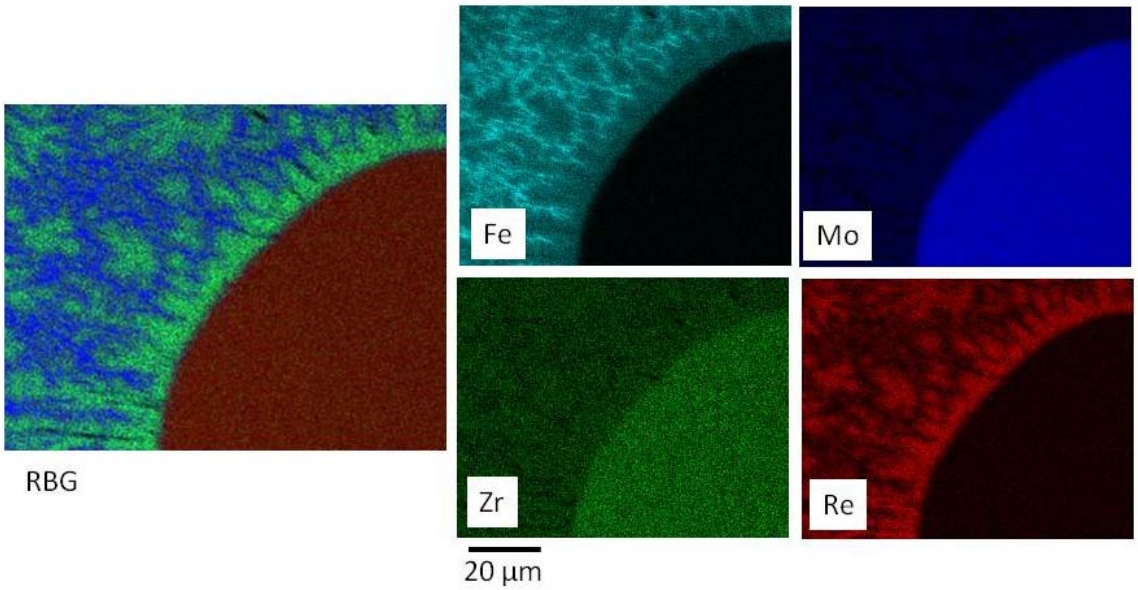

Figure 2.3 SEM analysis of FeMo-Re alloy; The RGB combination map used a mixture of elemental maps; iron, rhenium, and molybdenum. The instrument generated a map with Zr although Zr is not present in the alloy.

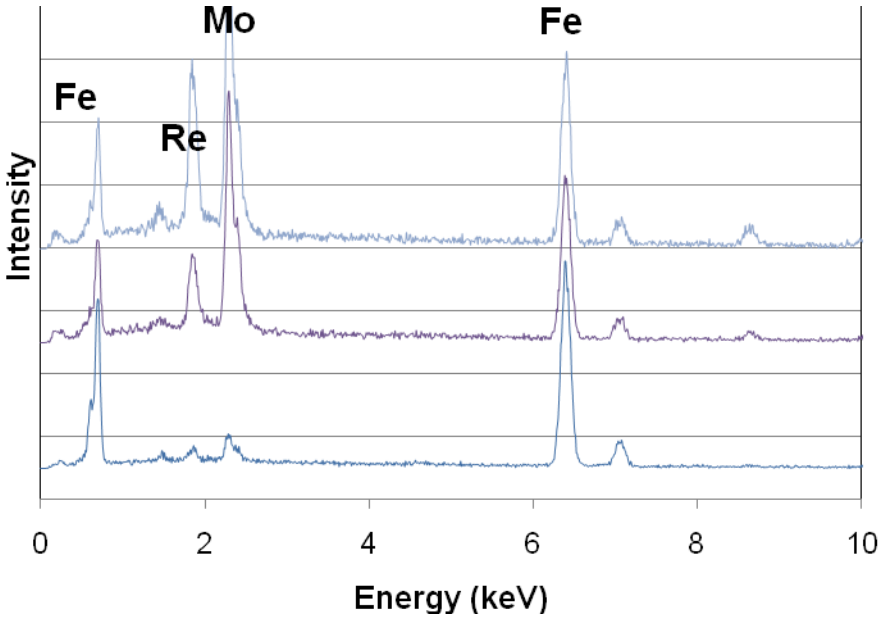

Figure 2.4 EDS of different phase compositions in the FeMo-Re alloy.

In Figure 2.4, EDS analyses from three different neighboring regions in the alloy are shown normalized to the iron Fe-K signal. The lower curve shows the ferrite composition, and the upper two spectra show two distinct compositions.

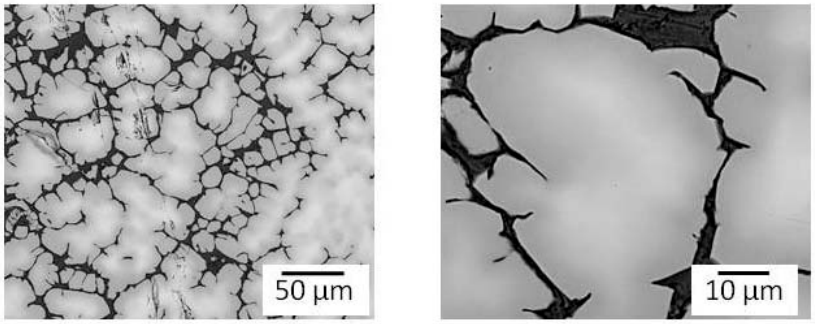

Figure 2.5 Backscattered images of FeMo-Re alloy showing a higher average Z material in the center of the Mo-Re rich regions.

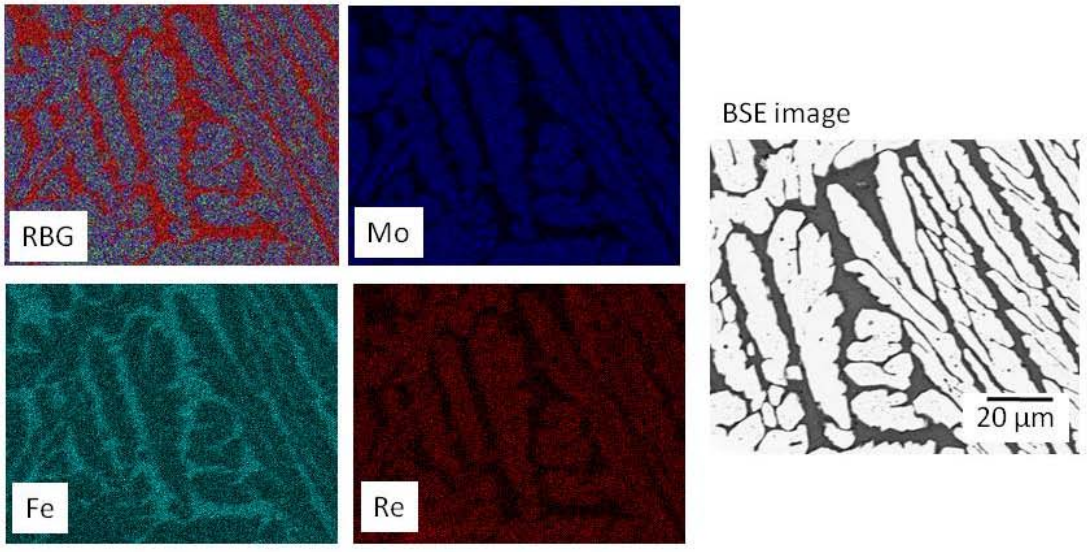

Figure 2.6 SEM analysis of FeMo-Re alloy, including a combination map, iron map, molybdenum map, rhenium map, and backscattered electron (BSE) image.

Backscattered images in Figure 2.5 of the metal waste form also reveal three phases, excluding the pure molybdenum phase. This additional rhenium-rich phase is only visible when the high Z

regions contrast is highlighted with BSE imaging. In the backscattered image in Figure 2.6, no significant contrast variation was observable and the rhenium rich region is not visible. In Figure 2.7, a series of spot analyses across the eutectic region show the variability in rhenium content but the presence of the third rhenium-rich phase is not as clear as in the backscattered images. Further work with TEM is required to determine if this is a separate phase or a solid solution. In Appendix B, relevant metal phases were selected and simulated electron diffraction patterns were generated.

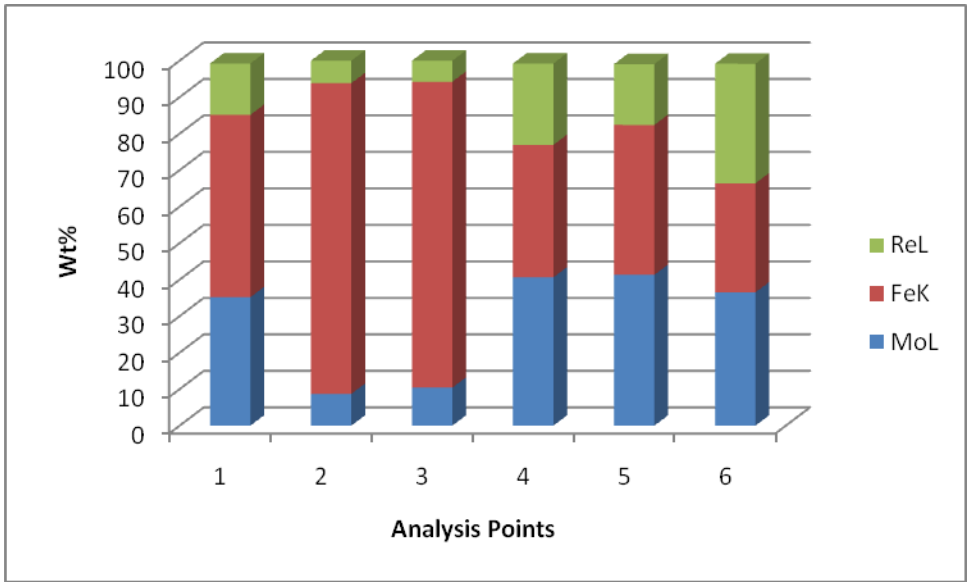

Figure 2.7 Series of data analyses showing variation in iron content.

2.2 TEM sample preparation

To produce samples suitable for TEM with radioactive materials, it is important to reduce the size of the samples as much as possible. An example of a TEM sample that was thinned using the tripod polisher technique is shown in Figure 2.7. These very small fragments were glued to a 3-mm diameter copper support ring for insertion into the TEM vacuum system. During polishing, it was clear that the softer iron (ferrite) is removed much more quickly than the intermetallic phases. As a result the material tends to fracture along the ferrite regions. Thus extreme care is required to produce electron transparent regions.

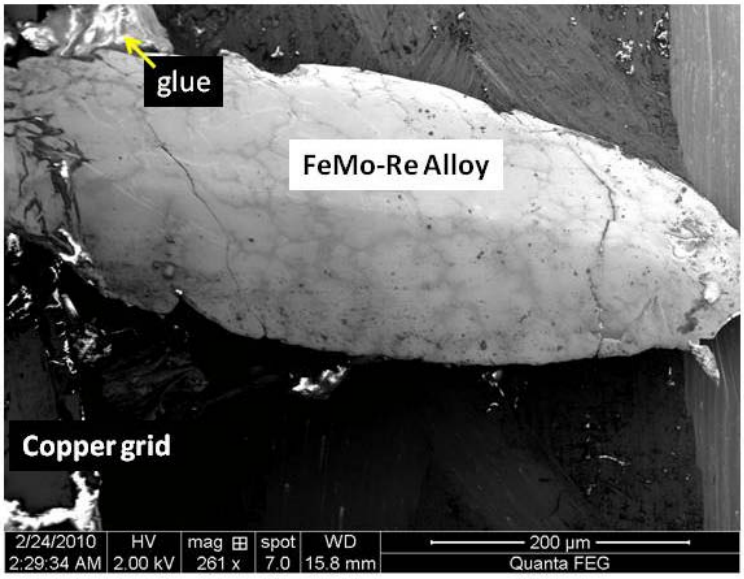

Figure 2.8 SEM image of specimen to be examined with TEM.

3. X-ray Diffraction

Profile fit

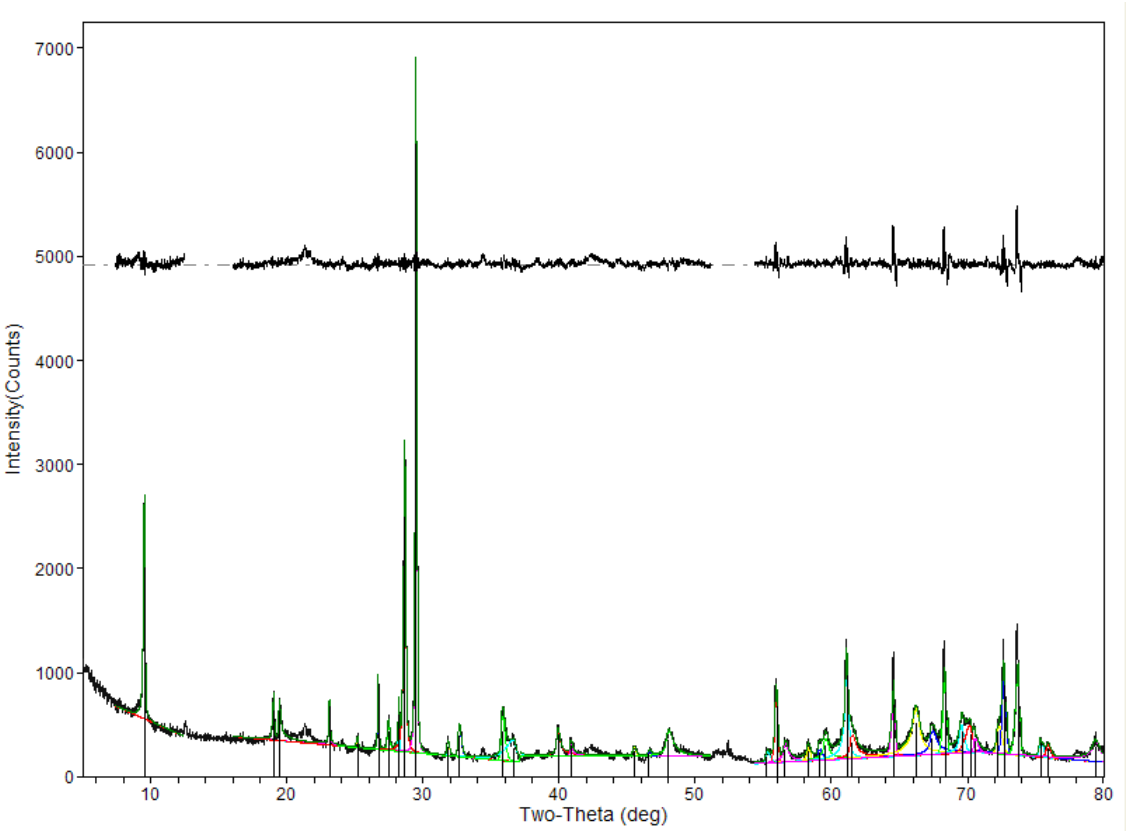

Profile fitting of the observed powder pattern.

The list below is obtained via this fit.

R = 15.53%

2-Theta	D	height	area	area %	FWHM
9.536	9.2667	1469	13349	34.8	0.122
19.053	4.6544	311	2690	7	0.14
19.44	4.5624	302	7608	19.8	0.139
23.15	3.839	394	3196	8.3	0.066
25.216	3.5289	72	551	1.4	0.135
26.725	3.333	646	3095	8.1	0.072
27.483	3.2427	207	2242	5.8	0.182
28.251	3.1563	378	2083	5.4	0.076
28.676	3.1105	2273	24593	64.1	0.151
29.503	3.0252	5868	38352	100	0.094
31.847	2.8077	102	1173	3.1	0.203
32.658	2.7398	219	3175	8.3	0.257
35.829	2.5043	300	5456	14.2	0.323
36.671	2.4486	144	9709	25.3	0.904
39.908	2.2572	221	7380	19.2	0.228
40.843	2.2076	119	2391	6.2	0.135
45.509	1.9916	69	895	2.3	0.229
46.6	1.9474	42	500	1.3	0.211
48.028	1.8928	177	8967	23.4	0.585
55.238	1.6616	81	1554	4.1	0.342
56.007	1.6406	569	6607	17.2	0.206
56.591	1.625	146	5686	14.8	0.367
58.315	1.581	113	1629	4.2	0.198
59.081	1.5624	93	1751	4.6	0.268
59.577	1.5505	166	8447	22	0.35
61.155	1.5142	825	16618	43.3	0.2
61.499	1.5066	180	10093	26.3	0.412
64.638	1.4408	519	6983	18.2	0.239
66.218	1.4102	324	20996	54.7	0.621
67.39	1.3885	176	10440	27.2	0.508
68.371	1.3709	612	7769	20.3	0.225
69.621	1.3494	220	5889	15.4	0.3
70.223	1.3393	189	6074	15.8	0.569
70.531	1.3341	132	1908	5	0.229
72.248	1.3066	219	4570	11.9	0.364
72.714	1.2994	680	8944	23.3	0.233
73.764	1.2835	680	10898	28.4	0.284
75.386	1.2598	154	1934	5	0.223
75.962	1.2517	109	1867	4.9	0.305
79.415	1.2057	164	9245	24.1	0.571

Orthorhombic: Pnma (62), Z=1
CELL: 4.35321 x 9.22283 x 18.59939 <90.0 x 90.0 x 90.0> Vol=746.7

R=46.77%
This unit cell does not account for all the peaks, and it is shifted.

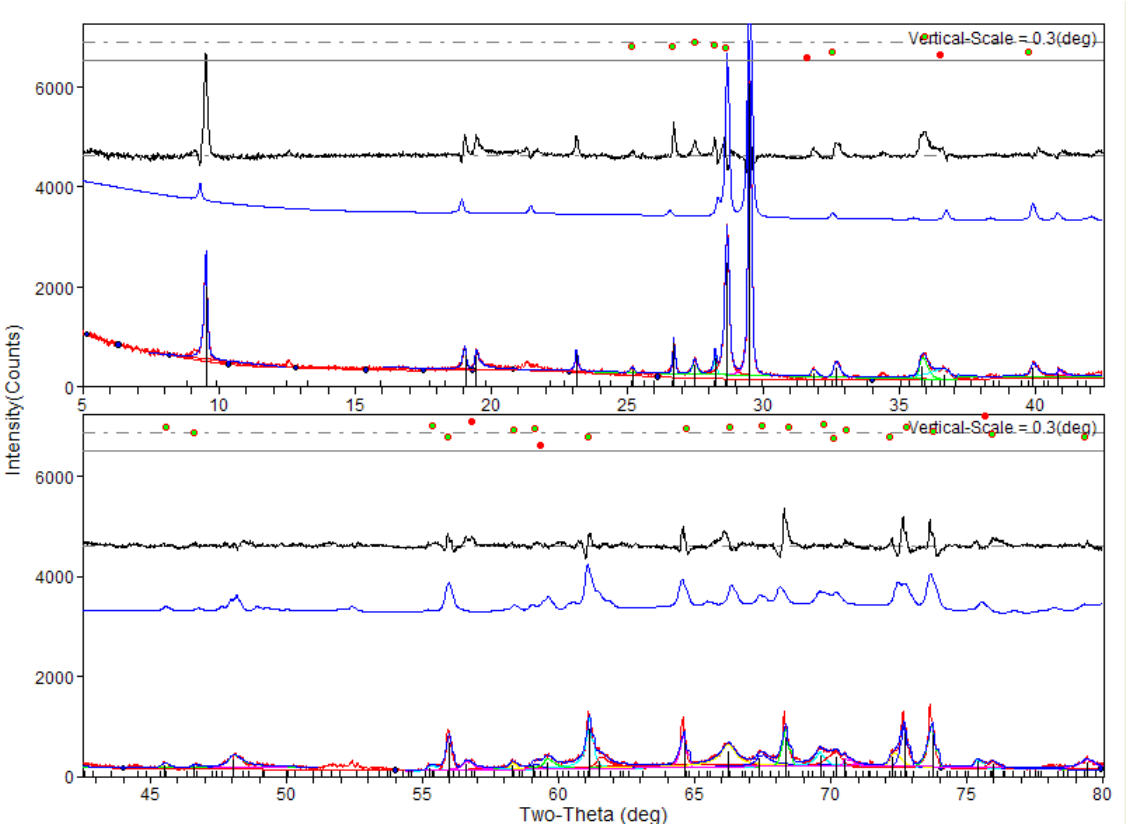

The refinement of the orthorhombic unit cell presented above. Red line – bottom is the observed and profile fitted powder pattern; the blue line is the simulated based on the cell, e.g. orthorhombic, black line- the difference between the observed and the calculated.

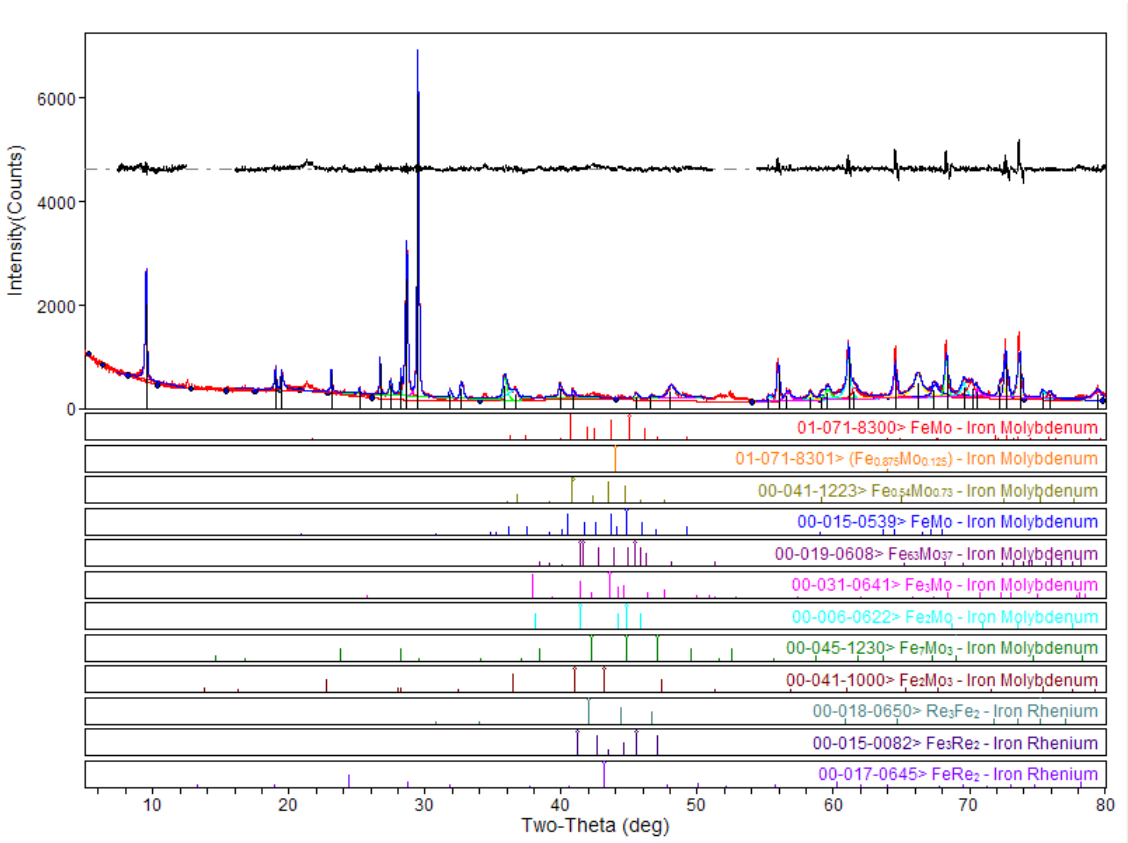

The observed powder pattern against some Fe/Mo and Fe/Re alloys.

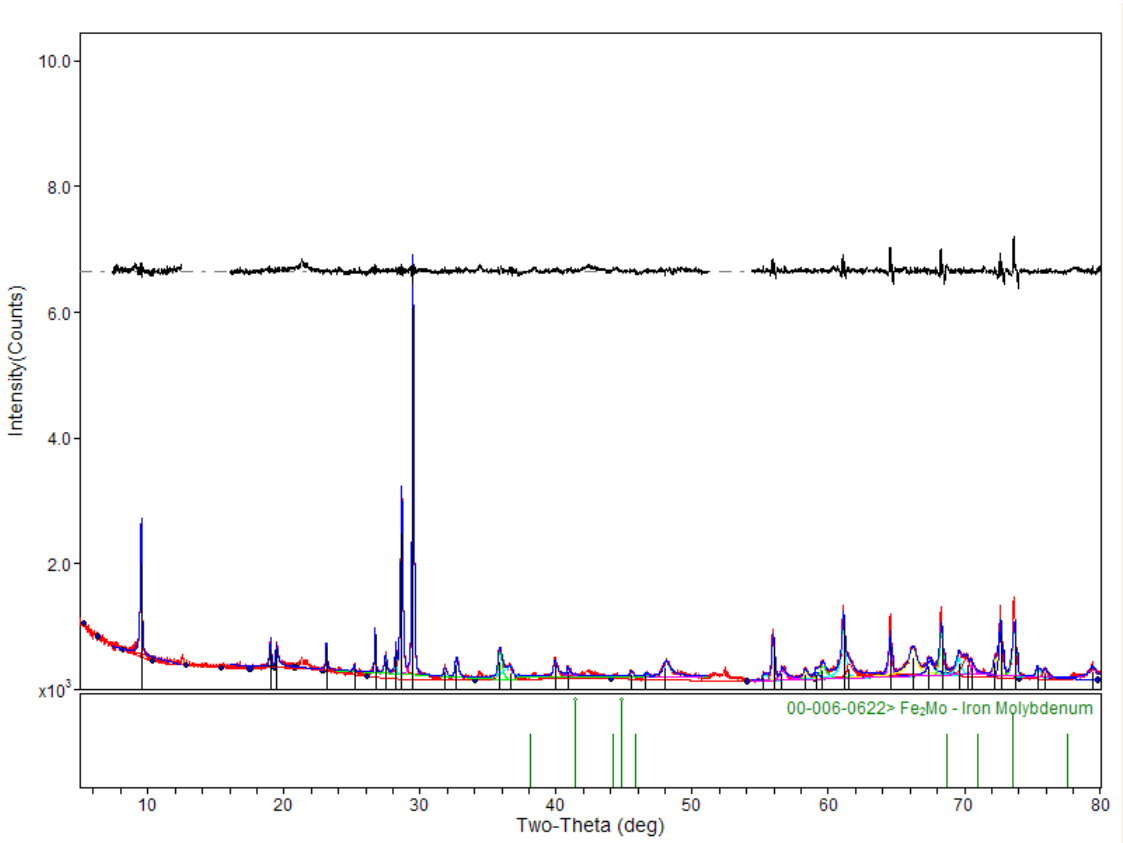

XRD data and the Fe2Mo phase.

Hexagonal: P63/mmc (194), Z=4
CELL: 9.38375 x 9.38375 x 18.6865 <90.0 x 90.0 x 120.0> Vol=1425.0
R=45.29%

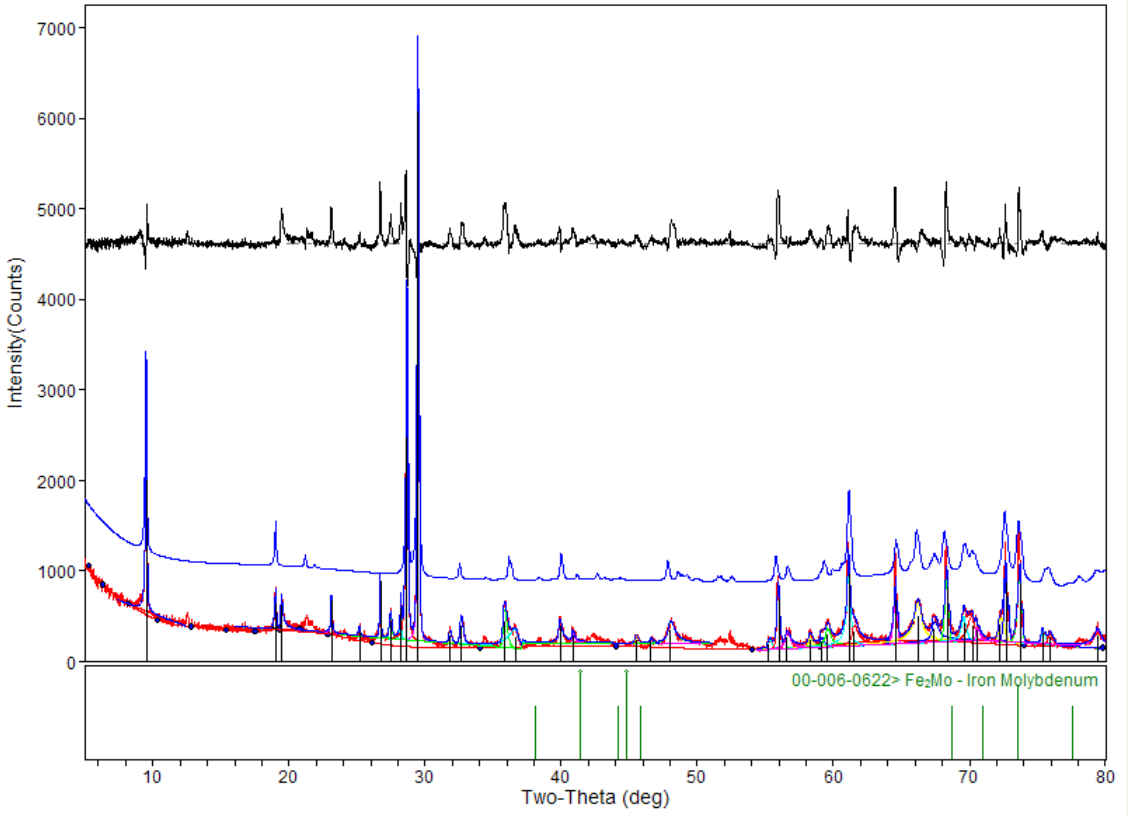

Raw XRD data – red line; simulated based on the hexagonal cell above – blue line; black line – the difference between the observed and the calculated data (based on the cell above).

4. CONCLUSIONS

The FeMo-Re alloy exhibited four phases. The molybdenum-bearing composition occurs as large separate phase. Based on composition, this molybdenum-rich phase does not appear to be un-melted molybdenum. The rhenium-rich and the rhenium-poor regions dominate the rest of the material. Inter-dispersed ferrite occurs throughout the remainder of the material. This FeMo-Re alloy along with the FeMo-Tc alloy will be examined in more detail as soon as the TEM instrument is available.

5. REFERENCES

Abraham, D.P., Richardson Jr., J.W., and McDeavitt, S.M. 2001. "Microscopy and Neutron Diffraction Study of a Zirconium-8wt% Stainless Steel Alloy." *Journal of Materials Science 36*, 5143-5154.

Ebert, W. 2009. *A Strategy for Conditioning TRUEX Raffinate Waste Form Immobilization*. AFCI-SUI-WAST-WAST-MI-DV-2009-000001.

Frank, S., O'Holleran, T., and Hahn, P. 2009. *Composition of Tc-Fe Alloy Produced for Testing*, FCRD-WAST-000011.

Gelles, D.S., Ermi, R.M., Buck, E.C., Seffens, R.J., and Chamberlin, C.E. 2009. Technetium Waste Form Development- Progress Report. Pacific Northwest National Laboratory report PNNL-18055.

ACKNOWLEDGEMENTS

The work summarized in this report was conducted at Pacific Northwest National Laboratory and at the University of Nevada-Las Vegas. Programmatic guidance provided by T. Todd (INL), J. Vienna (PNNL), and S. Lesica (DOE) is also gratefully acknowledged. Reviews by D. M. Strachan, M. W. Urie, and B. D. Hanson are also acknowledged.

Appendix A

Quality Assurance Standards

Magnification Scale

The magnification of the instrument was checked with a NIST standard. The instrument indicated magnification was within 1% of the expected value. The energy scale was checked by looking at high and low energy x-rays from known materials.

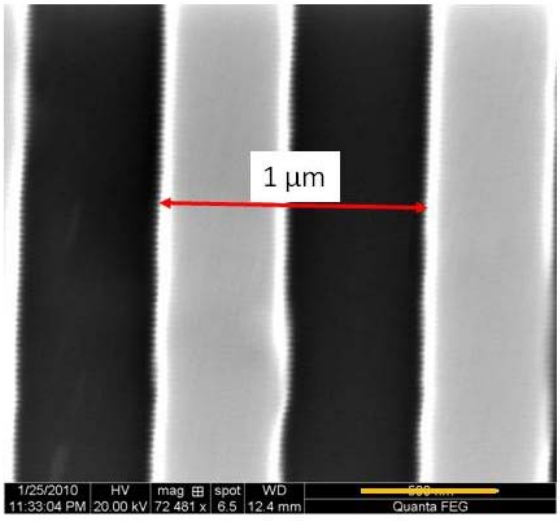

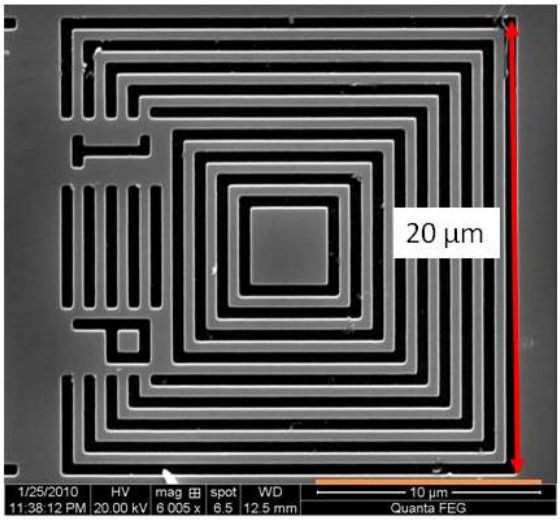

Appendix B

Fe-Mo System

Fe_2Mo –Hexagonal (P63/mmc) (intermetallic phase)
a= 4.724 Å, **c**=7.725 Å
Atomic Positions
Fe (0.33, 0.66, 0)
Fe (0.66, 0.33, 0.5)
Mo (0.33, 0.66, 0.375)
Mo (0.66, 0.33, 0.875)

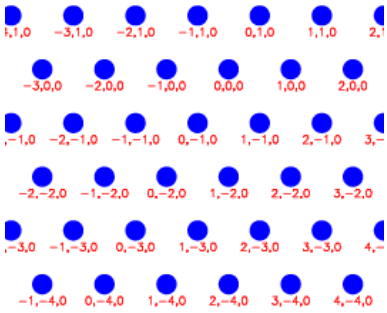

Simulated Electron Diffraction pattern **B**[0001]

FeMo –Tetragonal (P42/mnm)
a= 9.19 Å, **c**=4.81Å
Atomic Positions (each site is shared equally between Mo and Fe)
Fe (0, 0, 0)
Mo (0, 0, 0)
Fe (0.39875, 0.39875, 0)
Mo (0.39875, 0.39875, 0)
Fe (0.46351, 0.13131, 0)
Mo 0.46351, 0.13131, 0)

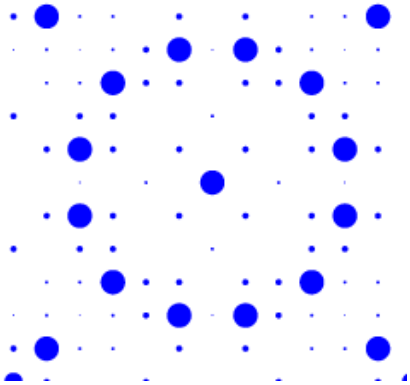

Simulated Electron Diffraction pattern **B**[001]